Chapter

Ru Complex Ion Induces Anomalous Enhancement of Electrochemical Charge Transfer

Huanwen Han, Kazuyuki Nobusawa, Fumie Takei, Ting-Chieh Chu, Noriyasu Hashida and Ichiro Yamashita

Abstract

Electrochemical impedance spectroscopy (EIS) is a highly sensitive observation technique to detect the state of electrode surfaces in solution. A small amount of $[Ru(bpy)_2DPPZ]^{2+}$, a well-known DNA intercalator and fluorescent light switch, has been found to abnormally increase the charge transfer of the mediator $[Fe(CN)_6]^{3-/4-}$ at the surface of carbon electrodes. When a very small amount of the Ru complex is added to the EIS solution, a large impedance decrease occurs. This phenomenon is caused by the carbon electrode, the mediator $[Fe(CN)_6]^{3-/4-}$ and $[Ru(bpy)_2DPPZ]^{2+}$. No other agents are necessary. By adding $[Fe(CN)_6]^{3-/4-}$ and a very small amount of $[Ru(bpy)_2DPPZ]^{2+}$ to the PCR solution, EIS measurements using a PVA-coated carbon electrode could monitor PCR progress in real-time as an increase in impedance.

Keywords: electrochemical impedance spectroscopy (EIS), $[Ru(bpy)_2DPPZ]^{2+}$, hexacyanoferrate, $[Fe(CN)_6]^{3-/4-}$, PCR, carbon electrode

1. Introduction

We are investigating electrochemical biosensors. Electrochemical biosensors have attracted researchers' attention because of their ability to operate under physiological solution conditions and biochemical high salt concentration solutions, simple configuration, and easy handling. In the electrochemical sensor, three electrodes, the working electrode (WE), the counter electrode (CE), and the reference electrode (RE), are immersed in the solution to be measured and detect changes in the charge transfer between redox mediators added to the measurement solution and the working electrode. A highly sensitive sensor can be realized by detecting changes in impedance between WE and CE. Hexacyanoferrate, $[Fe(CN)_6]^{3-/4-}$, of a few mM is often used as a redox mediator. The design of sensor systems varies widely, and to date, a variety of electrochemical biosensors have been proposed and studied [1–9].

We have been applying this electrochemical biosensor for real-time detection of polymerase chain reaction (PCR). PCR is a technique that amplifies the dsDNA of a target by doubling and used for detection of infectious viruses [10, 11], identification of viruses and bacteria [12, 13], diagnosis of tumors [14], gene expression

analysis [15] and single nucleotide polymorphisms [16]. It is usual that real-time PCR detection has been realized using a fluorescent dye and optics-based sensing method. However, conventional PCR detection requires a delicate and bulky optical fluorescence measurement system, and heavy equipment, which make the PCR device fragile, not portable, and expensive. Replacing the optics with a small electrical circuit should make PCR robust, compact, and cost-effective. It can be concluded that the use of an electrochemical sensor would be quite advantageous. Although there have been reports of electrochemical real-time PCR detection (quantitative PCR, qPCR) using voltammetry measurement techniques and EIS measurement methods [17–24], we have devised a completely new PCR detection system based on the simple EIS method, but introducing the idea of adding a small amount of a second mediator.

2. Electrochemical impedance spectroscopy (EIS)

We applied electrochemical impedance spectroscopy (EIS) as the biosensor detection technique. Three electrode system was employed, a working electrode (WE) a counter electrode (CE), and a reference electrode (RE), which are immersed into the solution, and the impedance between the WE and a CE is measured by applying AC voltage of about 10 mV with sweeping frequency. **Figure 1**(**a**) [25–32].

When the current due to the redox reaction is measured, Nyquist plot of the complex impedance is a combination of a semicircle and a straight line with a 45-degree slope (**Figure 1**(**b**)). This spectrum can be interpreted by Randall's equivalent circuit (**Figure 1**(**a**)), which consists of the charge transfer resistance of the electrode surface (Rct), the Warburg impedance due to mediator diffusion in the low-frequency range (Rw), the electric double layer capacitance of the electrode surface (Cdl) and the solution resistance (Rs). The semicircle is produced from the parallel junction of Rct and Cdl, and its diameter is approximately equal to Rct. Depending on the solution state, the charge transfer between the mediator and the electrode changes, resulting in a change in Rct which is the sensor output. The straight line with a 45-degree slope in the low-frequency region is the Warburg impedance.

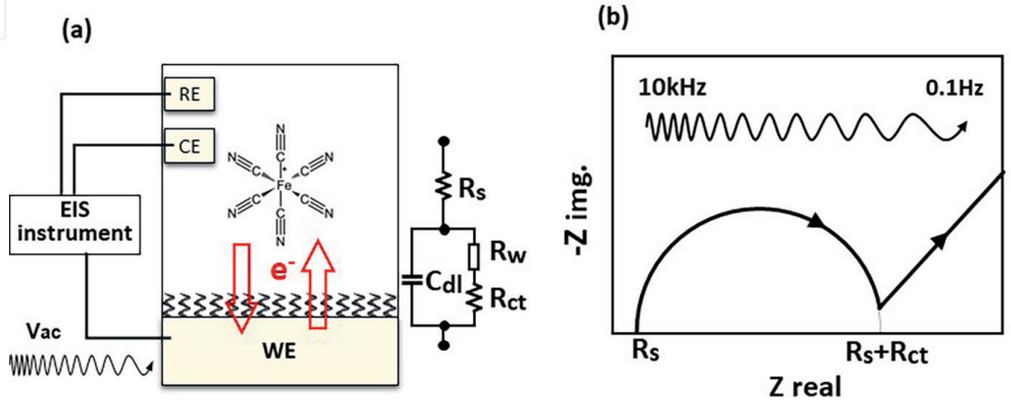

Figure 1.
(a) Schematic drawing of charge transfer between hexacyanoferrate, $[Fe(CN)_6]^{3-/4-}$ mediator, and working electrode (WE) with Randall equivalent circuit. (b) A typical Nyquist plot of electrochemical impedance spectroscopy (EIS).

3. $[Ru(bpy)_2DPPZ]^{2+}$ in the electrochemistry; search for the mediator of PCR

Our first step was to find a mediator molecule that would act as a mediator and intercalator of dsDNA simultaneously. As the PCR progresses, the dsDNA intercalates the mediator, resulting in an increase in Rct and allowing the PCR to be monitored in real time. We have selected $[Ru(bpy)_2DPPZ]^{2+}$, a derivative of $[Ru(bpy)_3]^{2+}$ that interacts with dsDNA and acts as a mediator. $[Ru(bpy)_2DPPZ]^{2+}$ was reported as a strong intercalator [33]. It binds mainly to the small groove of dsDNA, plugging the DPPZ portion between planar DNA base pairs [34, 35]. $[Ru(bpy)_2DPPZ]^{2+}$ also acts as an optical switch for double helical DNA with high luminescence sensitivity [33, 36]. It has therefore been studied in detail in chemosensors for the detection of luminescent signals. However, there have been few reports on the electrochemical properties.

First, cyclic voltammogram (CV) measurements were performed to investigate the electrochemical application of $[Ru(bpy)_2DPPZ]^{2+}$. **Figure 2** shows the measurement setup (Gamry. Instruments). The working electrodes of glassy carbon (GC) were polished with 1 μm of diamond paste and 50 nm aluminum oxide particles for 5 min each and then sonicated in ethanol and pure water for 5 min each. Pt wire was used for CE. The scan speed was 100 mV/sec and the potential range was -1 V to 1 V. (The same setting was used for the following measurements.) A solution of 10 mM Tris (pH 8.0) + 50 mM KCl + 1.5 mM $MgCl_2$ (PCRi) was used as the basic solution. **Figure 3(a)** shows the CV measurement result when 1 mM $[Ru(bpy)_2DPPZ]^{2+}$ was added. The redox peaks of $[Ru(bpy)_2DPPZ]^{2+}$ were observed in the negative potential region. The potential difference of the redox peaks (ΔEp) was large, suggesting that good charge transfer was not expected. For comparison, the CV, when 1 mM $[Fe(CN)_6]^{3-/4-}$ was added to the PCRi solution is shown in **Figure 3(b)**. The ΔEp was about 170 mV, suggesting that charge transfer is sufficiently rapid.

Next, EIS measurements were performed with 10 mVac and 1 kHz ~ 0.1 Hz in the PCRi solution. (The same conditions were used for the following EIS experiments). **Figure 3(e)** shows the results. The spectrum was a line extending almost vertically. The line was determined to be part of a semicircle with an extremely large Rct, and the Rct could be at least several hundred kΩ. This result indicated that the mediator function of $[Ru(bpy)_2DPPZ]^{2+}$ was low, which was initially expected.

Since 1 mM $[Ru(bpy)_2DPPZ]^{2+}$ alone did not provide sufficiently good charge transfer, we investigated whether the addition of 1 mM $[Fe(CN)_6]^{3-/4-}$, to this solution would lower the Rct resistance. **Figure 3(c)** shows the CV measurement results. The

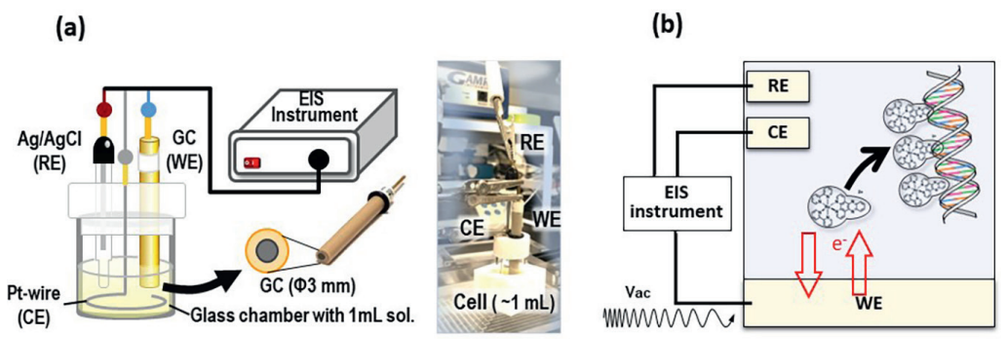

Figure 2.
(a) Schematic drawings of electrochemical measurement setting (3-electrode system) and a photo. (b) Desirable $[Ru(bpy)_2DPPZ]^{2+}$ function as a mediator and intercalator.

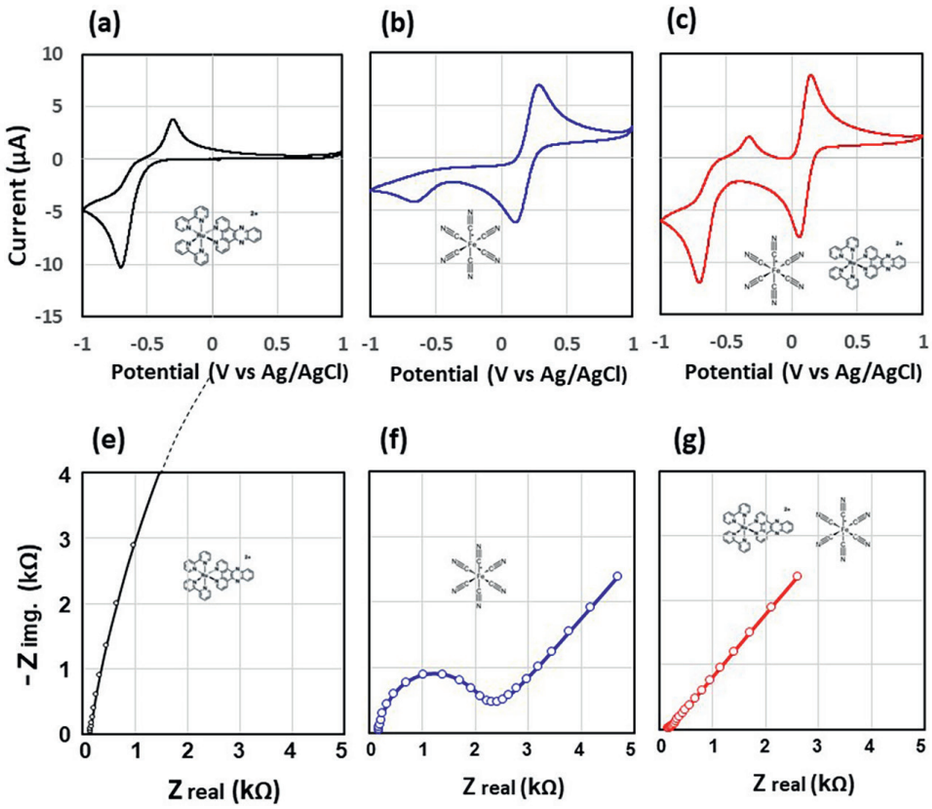

Figure 3.
CV and EIS results were obtained using PCRi solution with (a)(e) 1 mM $[Ru(bpy)_2DPPZ]^{2+}$, (b)(f) 1 mM $[Fe(CN)_6]^{3-/4-}$, (c)(g) both ions. The size of the CG-WE was ϕ3 mm.

obtained CV characteristics were similar to the sum of the peak position and current for 1 mM $[Ru(bpy)_2DPPZ]^{2+}$ and 1 mM $[Fe(CN)_6]^{3-/4-}$, except that the redox peaks of $[Fe(CN)_6]^{3-/4-}$ showed a substantial change. The redox peak current was larger and ΔEp was much narrower, about 90 mV. The result suggested that the charge transfer of $[Fe(CN)_6]^{3-/4-}$ mediator was enhanced by 1 mM $[Ru(bpy)_2DPPZ]^{2+}$ significantly. EIS measurements also confirmed this charge transfer enhancement (**Figure 3(f)**, **(g)**). The spectra showed that the semicircle in **Figure 3(f)** decreased to the extent that the semicircle is almost unobservable (**Figure 3(g)**). Rct decreased significantly.

From these measurements, we concluded that $[Ru(bpy)_2DPPZ]^{2+}$ alone cannot be used as a mediator for EIS measurements. However, there was a new finding that $[Ru(bpy)_2DPPZ]^{2+}$ greatly enhanced the charge transfer of $[Fe(CN)_6]^{3-/4--}$.

4. Qualitative evaluation of charge transfer enhancement by $[Ru(bpy)_2DPPZ]^{2+}$

We studied the dependence of charge transfer enhancement on the concentration of $[Ru(bpy)_2DPPZ]^{2+}$ by EIS. EIS measurements were repeated every 5 min and for the first 60 min, we waited for the equilibration, "termination" of the glassy carbon WE in a PCRi +1 mM $[Fe(CN)_6]^{3-/4-}$. After stabilization, $[Ru(bpy)_2DPPZ]^{2+}$ was added stepwise every 30 min to a final concentration of 1, 3, 5, 10, 30, 50, 100, 300, 500 nM, 1, 2, 3, 5, 10 μM, and 1 mM. After each addition, EIS measurements were performed every 5 min. All obtained EIS spectra were then fitted with a Randle equivalent circuit, and Rcts were

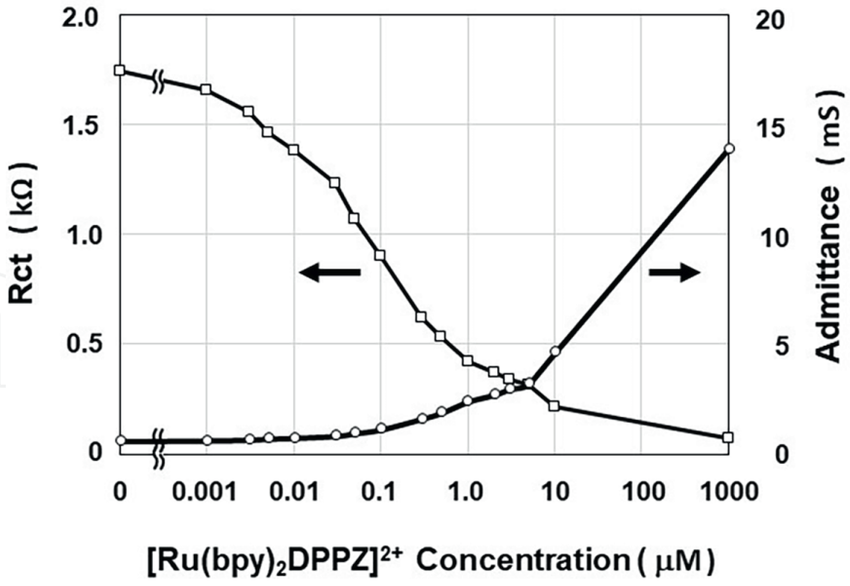

Figure 4.
The dependence of Rct and 1/Rct on $[Ru(bpy)_2DPPZ]^{2+}$ concentration. The charge transfer resistances were extracted from EIS spectra.

calculated using software (Gamry. Instruments). The obtained Rct and 1/Rct were plotted against $[Ru(bpy)_2DPPZ]^{2+}$ concentration in **Figure 4**.

Rct started to decrease from 1 nM concentration. At 100 nM concentration, Rct was reduced by half and about 1/4 at 1 μM. The Rct continued to decrease to approximately 1/25 at 1 mM concentration. In terms of admittance, Rct increases from 0.57 mS to 13.9 mS, suggesting that this phenomenon is not saturated even at concentrations above 10 μM. This result indicates that the charge enhancement effect of the $[Ru(bpy)_2DPPZ]^{2+}$ occurs over a wide range of concentrations from 1 nM to 1 mM, when the concentration of the $[Fe(CN)_6]^{3-/4-}$ mediator is 1 mM.

5. Charge transfer enhancement arises from the combination of $[Ru(bpy)_2DPPZ]^{2+}$, $[Fe(CN)_6]^{3-/4-}$ and carbon electrode

The Ru effect was found to occur with very small amounts of Ru complex ions, but the base solution contained 10 mM Tris pH 8.0, 50 mM KCl, and 1.5 mM $MgCl_2$.

We first removed the ionic substances 50 mM KCl and 1.5 mM $MgCl_2$ from the solution and performed EIS measurements. After stabilization, 0.5 μM and 1.0 μM $[Ru(bpy)_2DPPZ]^{2+}$ were added in sequence and EIS measurements were performed. **Figure 5(a)(e)** shows the change in EIS spectra and Rct decrease after the addition of $[Ru(bpy)_2DPPZ]^{2+}$. Upon addition of 0.5 μM $[Ru(bpy)_2DPPZ]^{2+}$, the Rct decreased rapidly and the Rct further decreased to almost 1/15 with f 1.0 μM. This result indicates that these KCl and $MgCl_2$ ions are not related to the charge transfer enhancement effect.

Next, the buffer, 10 mM Tris pH 8.0 was replaced with 10 mM phosphate buffer pH 8.0, and similar EIS measurements were performed. **Figure 5(b)(f)** shows the results. The addition of $[Ru(bpy)_2DPPZ]^{2+}$ rapidly decreased Rct to about 1/15 at 1 μM, similar to the Tris buffer, indicating that Tris buffer did not have the effect either.

To see the effect of pH, we also performed an experiment using 10 mM phosphate buffer pH 6.5 + 1.0 mM $[Fe(CN)_6]^{3-/4-}$. **Figure 5(c)(g)** shows the results. As in the case of pH 8.0, a sharp decrease in Rct was observed.

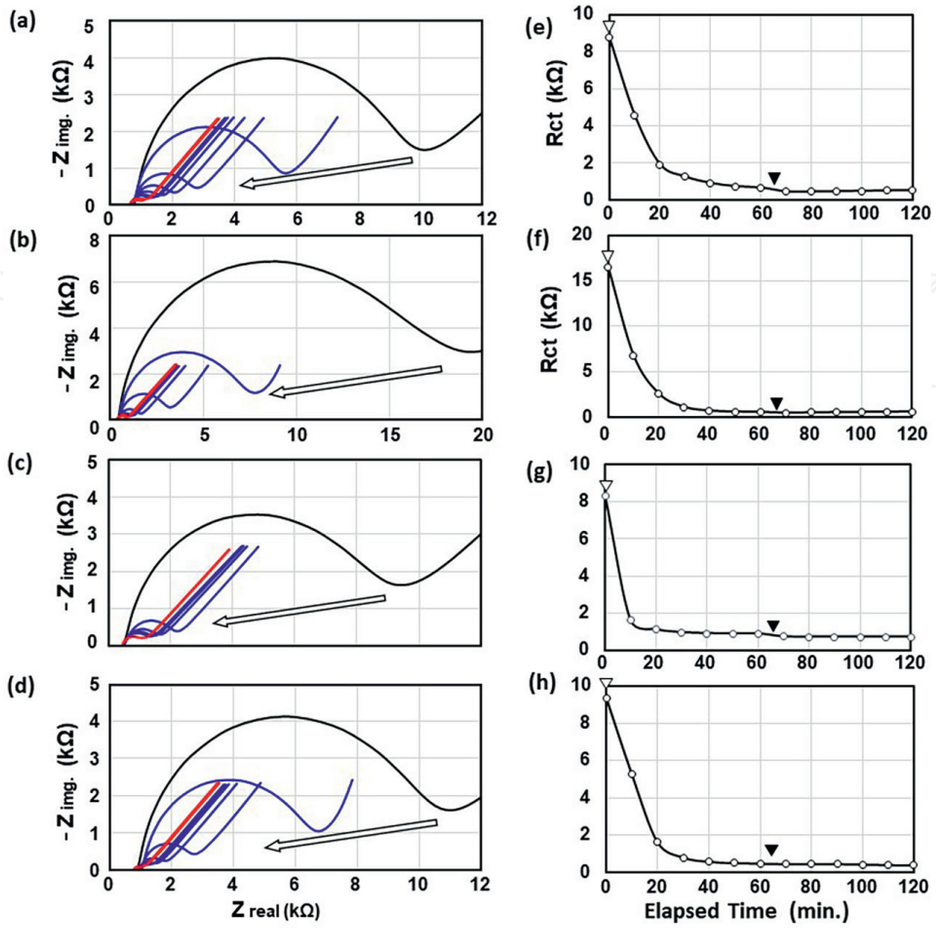

Figure 5.
EIS spectra and time-dependency of Rct without (black), with 0.5 μM (blue) and 1.0 μM (red) $[Ru(bpy)_2DPPZ]^{2+}$ in (a) (e)10 mM Tris pH 8.0 and 1.0 mM $[Fe(CN)_6]^{3-/4-}$, (b) (f) 10 mM phosphate buffer pH 8.0 and 1.0 mM $[Fe(CN)_6]^{3-/4-}$, and (c) (g) 10 mM phosphate buffer pH 6.5 and 1.0 mM $[Fe(CN)_6]^{3-/4-}$, (d) (h) 1.0 mM $[Fe(CN)_6]^{3-/4-}$. EIS spectra were drawn every 10 min. The white (△) and black (▲) mark the time points at which 0.5 μM and 1 μM of $[Ru(bpy)_2DPPZ]^{2+}$ were added, respectively.

Finally, the buffer was removed. EIS measurement was performed with only 1 mM$[Fe(CN)_6]^{3-/4-}$ in pure water. The pH of the solution was about 6.5. **Figure 5(d)(h)** shows the EIS results. Even in a simple solution of 1 mM $[Fe(CN)_6]^{3-/4-}$ alone, the addition of $[Ru(bpy)_2DPPZ]^{2+}$ ions promotes charge transfer, resulting in a significant decrease in Rct, which eventually reaches less than 1/20 of Rct.

Figure 5(e)-(h) shows the time dependence of Rct calculated from EIS measurements. In all cases, the Rct decrease was completed in about 20 minutes.

From these results, we can conclude that the newly discovered charge transfer enhancement effect is caused by the combination of $[Ru(bpy)_2DPPZ]^{2+}$, $[Fe(CN)_6]^{3-/4-}$, and a carbon electrode. The $[Ru(bpy)_2DPPZ]^{2+}$ enhances the charge transfer between the carbon electrode and $[Fe(CN)_6]^{3-/4-}$ by some mechanism. This effect is also observed at various carbon electrodes [37].

6. PCR monitoring by EIS

Based on the new findings, we conceived the idea of applying the charge transfer enhancement effect by the DNA intercalator to the real-time monitoring of PCR

[38]. In PCR, forward and revers primers of ssDNA are annealed to the DNA template, and DNA polymerase synthesizes dsDNA amplicons in heat cycles. Therefore, if $[Fe(CN)_6]^{3-/4-}$ and a small amount of $[Ru(bpy)_2DPPZ]^{2+}$ are added to the PCR solution and EIS measurement is performed using a carbon electrode, the progress of PCR can be monitored. The Rct would initially be low and as the PCR proceeds, the generated dsDNA would intercalate $[Ru(bpy)_2DPPZ]^{2+}$, and the Rct increases. The progress of PCR can be monitored by Rct.

To realize this monitoring method, we must first make a porous protective layer on the carbon electrode. We coated the carbon electrode with polyvinyl alcohol (PVA). Carbon electrodes were immersed in 0.1% PVA (30 k-51 kDa) for 1 hour and EIS measurements were performed in PCRi +1 mM $[Fe(CN)_6]^{3-/4-}$ solution, then 1 μM ssDNA (17 nt) and 1 μM dsDNA (60 bp) were added sequentially. The EIS spectrum remained almost unchanged from its initial shape, indicating that DNA adsorption was prevented (**Figure 6**).

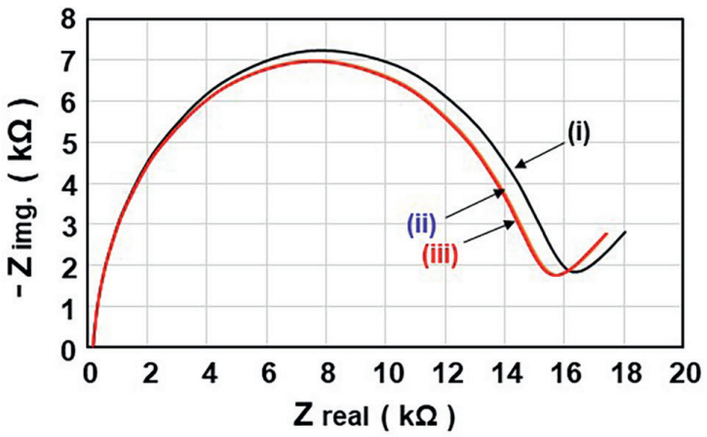

Figure 6.
EIS measurements using carbon electrode with PVA layer. (i) in PCRi + 1 mM, $[Fe(CN)_6]^{3-/4-}$ solution. (ii) after 1 μM ssDNA (17 nt) addition, (iii) after 1 μM dsDNA (60 bp) addition.

Integrating the results, PCR was performed; 3 mM $[Fe(CN)_6]^{3-/4-}$ and 5 μM $[Ru(bpy)_2DPPZ]^{2+}$ were added to the PCR solution, and PCR progress was monitored by EIS using a screen-printed carbon electrode. Template DNA concentrations were 100 ng/mL, 1 ng/mL, 10 pg/mL, and 0.1 pg/mL, and EIS measurements with a frequency range of 1 kHz to 0.5 Hz, open circuit potential, and 100 mVac were conducted during PCR extension steps.

All EIS spectra were fitted to a Randle equivalent circuit and Rcts were calculated. **Figure 7(a)** shows the change in Rct for each template DNA concentration versus heat cycle. Rcts were approximately 10–20 kΩ (See **Figure 7(d)**), however, its absolute value varied from sensor to sensor depending on the electrode preparation conditions, as is often the case [39]. To easily compare the results, all Rcts were normalized by setting the Rct at the eighth heat cycle as 1.0, and Rcts were overdrawn.

In the beginning, Rct increased gradually due to the adsorption of minute impurities on the electrode. Unlike this gradual increase, a clear abrupt increase in Rct occurred around 13, 21, 28, and 35 thermal cycles at DNA template concentrations of 100 ng/mL, 1 ng/mL, 10 pg/mL, and 0.1 pg/mL, followed by a gradual increase in Rct. This rapid increase in Rct is the result of the exponential amplification of the dsDNA amplicon and intercalation of $[Ru(bpy)_2DPPZ]^{2+}$.

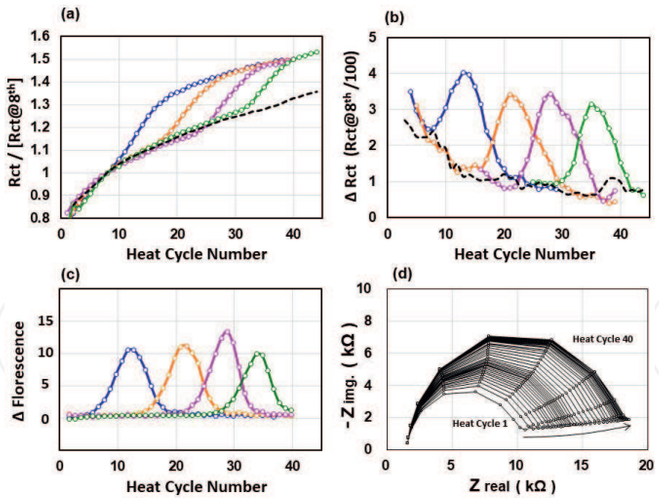

Figure 7.
Monitoring results of PCR with DNA template concentrations of 100 ng/mL, 1 ng/mL, 10 pg/mL, and 0.1 pg/mL (a) Rct calculated from EIS by fitting to the Randle circuit with constant phase element, (b) ΔRct; Rct increase at each heat cycle, and (c) optical fluorescence increase. Background without template DNA is shown as a broken black line. All data are three moving averages. (d) One example of changes in EIS spectra during PCR at the extension step. The Arrow indicates spectral changes along the heat cycle.

The change in Rct is more clearly confirmed by ΔRct, the increase in normalized Rct at each thermal cycle (**Figure 7(b)**). The vertical axis is 1/100th scale of the Rct@8th.

The more DNA template in the initial solution, the earlier by 7 cycles the heat cycle where the peak starts, increasing by seven cycles each. Theoretically, the number of amplicons would double with each cycle. The present results correspond well to the theoretical values. Gel electrophoresis of the PCR amplicon samples also confirmed that the target DNA was successfully amplified. It can be concluded that the inhibitory effect of the addition of 3 mM $[Fe(CN)_6]^{3-/4-}$ and 5 μM $[Ru(bpy)_2DPPZ]^{2+}$ is negligible. PCR monitoring with EIS was successfully demonstrated.

Optical PCR was performed in parallel using the same PCR solution (micPCR, Bio Molecular Systems, Australia). 20 μL of the solution was added with 1 U/L SYBR Gold (Toyobo Corporation), PCR was performed, and fluorescence was measured. **Figure 7(c)** shows the fluorescence intensity increase/cycle (Δfluorescence). Δflorescence showed a peak with 10 thermal cycle width. The peak positions by impedance and optical methods were in good agreement. The critical threshold cycle (Ct) was confirmed to be detectable by EIS.

The above results show that the electrochemical detection method which utilizes the anomalous charge transfer enhancement effect can monitor the progress of PCR in real time and realize quantitative PCR [38].

7. Conclusion

We proposed a new impedance detection method for real-time PCR based on EIS and demonstrated its practicality. The simplicity of this impedance detection method allowed us to fabricate qPCR with simple components and to realize a small, portable,

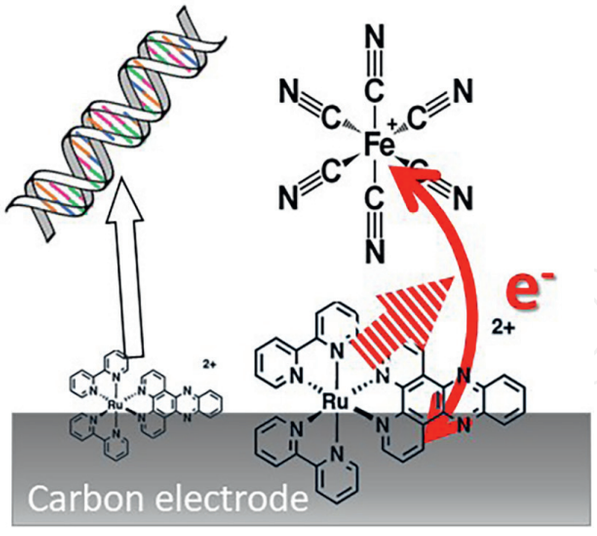

Figure 8.
A possible charge transfer enhancement mechanism and the relation with $[Ru(bpy)_2DPPZ]^{2+}$ and dsDNA. $[Ru(bpy)_2DPPZ]^{2+}$ adsorbs on the carbon electrode and enhances the charge transfer through the ligands.

robust, and inexpensive device. At present, the mechanism of this effect is not clear. It was known that $[Fe(CN)_6]^{3-/4-}$ is a surface-sensitive mediator, therefore, the effect may have been caused by interaction or specific adsorption of $[Ru(bpy)_2DPPZ]^{2+}$ on the basal or edge surfaces of the carbonaceous electrode, which facilitates charge transfer (see **Figure 8**). This effect is observed in a variety of carbon electrodes, including graphite, graphene, and screen-printed carbon, and is expected to be widely applied beyond this PCR application.

Acknowledgements

This research is partially supported by the Center of Innovation Program (Grant No. JPMJCE1310) and Core Research for Evolutional Science and Technology, CREST (Grant No. JPMJCR18I3) from Japan Science and Technology Agency, JST.

Conflict of interest

The authors declare no conflict of interest.

Author details

Huanwen Han[1], Kazuyuki Nobusawa[1,2], Fumie Takei[3],
Ting-Chieh Chu[1], Noriyasu Hashida[4] and Ichiro Yamashita[1*]

1 Graduate School of Engineering, Osaka University, Suita, Osaka, Japan

2 Textile Research Institute of Gunma, Kiryu, Japan

3 National Defense Medical College, Tokorozawa-shi, Saitama, Japan

4 Department of Ophthalmology, Osaka University Graduate School of Medicine, Suita, Osaka, Japan

*Address all correspondence to: yamashita@jrl.eng.osaka-u.ac.jp

References

[1] Huang Y, Xu J, Liu J, Wang X, Chen B. Disease-related detection with electrochemical biosensors: A review. Sensors. 2017;**17**(10):2375

[2] Naveen MH, Gurudatt NG, Shim YB. Applications of conducting polymer composites to electrochemical sensors: A review. Applied Materials Today. 2017;**9**:419-433

[3] Shao Y, Wang J, Wu H, Liu J, Aksay IA, Lin Y. Graphene based electrochemical sensors and biosensors: A review. Electroanalysis. 2010;**22**(10):1027-1036

[4] Wang Z, Dai Z. Carbon nanomaterial-based electrochemical biosensors: An overview. Nanoscale. 2015;**7**:6420-6431

[5] Barsan MM, Ghica ME, Brett CMA. Electrochemical sensors and biosensors based on redox polymer/carbon nanotube modified electrodes: A review. Analytica Chimica Acta. 2015;**881**:1-23

[6] Zhu C, Yang G, Li H, Du D, Lin Y. Electrochemical sensors and biosensors based on nanomaterials and nanostructures. Analytical Chemistry. 2015;**87**(1):230-249

[7] Saidur MR, AbdulAziz AR, Basirunbc WJ. Recent advances in DNA-based electrochemical biosensors for heavy metal ion detection: A review. Biosensors & Bioelectronics. 2017;**90**:125-139

[8] Li H, Liu X, Mu X, Genov R, Mason AJ. CMOS electrochemical instrumentation for biosensor microsystems: A review. Sensors. 2017;**17**(1):74

[9] Fujino Y, Nakamura R, Han H-W, Yamashita I, Shimizu T, Shingubara S, et al. Electrochemical impedance spectroscopy study of liposome adsorption and rupture on self-assembled monolayer: Effect of surface charge. Electroanalytical Chemistry. 2020;**878**:114572

[10] Faye O, Faye O, Diallo D, Diallo M, Weidmann M, Sall AA. Quantitative real-time PCR detection of Zika virus and evaluation with field-caught Mosquitoes. Virology Journal. 2013;**10**:311

[11] Park M, Won J, Choi BY, Lee CJ. Optimization of primer sets and detection protocols for SARS-CoV-2 of coronavirus disease 2019 (COVID-19) using PCR and real-time PCR. Experimental & Molecular Medicine. 2020;**52**:963-977

[12] Lehmann LE, Hunfeld K-P, Emrich T, Haberhausen G, Wissing H, Hoeft A, et al. A multiplex real-time PCR assay for rapid detection and differentiation of 25 bacterial and fungal pathogens from whole blood samples. Medical Microbiology and Immunology. 2008;**197**:313-324

[13] Kralik P, Ricchi M. A Basic Guide to Real Time PCR in microbial diagnostics: Definitions, parameters, and everything. Frontiers in Microbiology. 2017;**8**. Article 108

[14] Resnick KE, Alder H, Hagan JP, Richardson DL, Croce CM, Cohn DE. The detection of differentially expressed microRNAs from the serum of ovarian cancer patients using a novel real-time PCR platform. Gynecologic Oncology. 2009;**112**:55-59

[15] Spurgeon SL, Jones RC, Ramakrishnan R. High throughput gene expression measurement with real time

PCR in a microfluidic dynamic array. PLoS One. 2008;**3**:e1662

[16] Myakishev MV, Khripin Y, Hu S, Hamer DH. High-throughput SNP genotyping by Allele-specific PCR with universal energy-transfer-labeled primers. Genome Research. 2001;**11**:163-169

[17] Yeung SSW, Lee TMH, Hsing I-M. Electrochemistry-based real-time PCR on a microchip. Analytical Chemistry. 2008;**80**:363-368

[18] Deféver T, Druet M, Dequaire MR, Joannes M, Grossiord C, Limoges B, et al. Real-time electrochemical monitoring of the polymerase chain reaction by mediated redox catalysis. American Chemical Society. 2009;**131**:11433-11441

[19] Deféver T, Druet M, Evrard D, Marchal D, Limoges B. Real-time electrochemical PCR with a DNA intercalating redox probe. Analytical Chemistry. 2011;**83**:1815-1821

[20] Moreau M, Delile S, Sharma A, Fave C, Perrier A, Limoges B, et al. Detection of a few DNA copies by real-time electrochemical polymerase chain reaction. Analyst. 2017;**142**:3432-3440

[21] Chen J, Yang T, Jiao K, Gao H. A DNA electrochemical sensor with poly-L-lysine/single-walled carbon nanotubes films and its application for the highly sensitive EIS detection of PAT gene fragment and PCR amplification of NOS gene. Electrochimica Acta. 2008;**53**:2917-2924

[22] Wang L, Liu Q, Hu Z, Zhang Y, Wu C, Yang M, et al. A novel electrochemical biosensor based on dynamic polymerase-extending hybridization for E. coli O157:H7 DNA detection. Talanta. 2009;**78**:647-652

[23] Corrigan DK, Schulze H, Henihan G, Ciani I, Giraud G, Terry JG, et al. Impedimetric detection of single-stranded PCR products derived from methicillin resistant Staphylococcus aureus (MRSA) isolates. Biosensors & Bioelectronics. 2012;**34**:178-184

[24] Chen C-C, Lai Z-L, Wang G-J, Wu C-Y. Polymerase chain reaction-free detection of hepatitis B virus DNA using a nanostructured impedance biosensor. Biosensors & Bioelectronics. 2016;**77**:603-608

[25] Lasia A. In: Conway BE, Bockris JOM, White RE, editors. Modern Aspects of Electrochemistry No.32. Electrochemical Impedance Spectroscopy and its Applications. Boston, MA: Springer; 2002. pp. 143-248. DOI: 10.1007/0-306-46916-2_2

[26] Bogomolova A, Komarova E, Reber K, Gerasimov T, Yavuz O, Bhatt S, et al. Challenges of electrochemical impedance spectroscopy in protein biosensing. Analytical Chemistry. 2009;**81**(10):3944-3949

[27] Chang BY, Park SM. Electrochemical impedance spectroscopy. Annual Review of Analytical Chemistry. 2010;**3**:207-229

[28] Lisdat F, Schäfer D. The use of electrochemical impedance spectroscopy for biosensing. Analytical and Bioanalytical Chemistry. 2008;**391**:155

[29] Park JY, Park SM. DNA hybridization sensors based on electrochemical impedance spectroscopy as a detection tool. Sensors. 2009;**9**(12):9513-9532

[30] Randviir EP, Banks CE. Electrochemical impedance spectroscopy: An overview of bioanalytical applications. Analytical Methods. 2013;**5**:1098-1115

[31] Grossi M, Riccò BJ. Electrical impedance spectroscopy (EIS) for biological analysis and food characterization: A review. Journal of Sensors and Sensor Systems. 2017;**6**:303-325

[32] Li X, Zhang Y, Chen H, Sun J, Feng F. Protein nanocages for delivery and release of luminescent ruthenium (II) polypyridyl complexes. ACS Applied Materials & Interfaces. 2016;**8**:22756-22761

[33] Friedman A, E, Chambron J-C, Sauvage J-P, Turro NJ, Barton JK. Molecular "Light Switch" for DNA: $Ru(bpy)_2(dppz)^{2+}$. Journal of the American Chemical Society. 1990;**112**:4960-4962

[34] Li G, Sun L, Ji L, Chao H. Ruthenium (II) complexes with dppz: From molecular photoswitch to biological applications. Dalton Transactions. 2016;**45**:13261-13267

[35] Song H, Kaiser J, Barton JK. Crystal structure of Δ-$[Ru(bpy)_2dppz]^{2+}$ bound to mismatched DNA reveals side-by-side metalloinsertion and intercalation. Nature Chemistry. 2012;**4**:615-620

[36] Brennaman MK, Alstrum-Acevedo JH, Fleming CN, Jang P, Meyer TJ, Papanikolas JM. Turning the $[Ru(bpy)_2dppz]^{2+}$ light-switch on and off with temperature. Journal of the American Chemical Society. 2002;**124**:15094-15098

[37] Han H, Nobusawa K, Yamashita I. Anomalous enhancement of electrochemical charge transfer by a Ru complex ion intercalator. Analytical Chemistry. 2022;**94**(2):571-576

[38] Nobusawa K, Han H, Takei F, Chu T, Hashida N, Yamashita I. Electrochemical impedimetric real-time polymerase chain reactions using anomalous charge transfer enhancement. Analytical Chemistry. 2022;**94**(22):7747-7751

[39] McCreery RL. Advanced carbon electrode materials for molecular electrochemistry. Chemical Reviews. 2008;**108**:2646-2687